ACS APPLIED MATERIALS & INTERFACES

Research Article

www.acsami.org

Highly Adhesive and Soluble Copolyimide Binder: Improving the Long-Term Cycle Life of Silicon Anodes in Lithium-Ion Batteries

Jaecheol Choi,[†,‡,⊥] Kyuman Kim,[†,⊥] Jiseon Jeong,[†] Kuk Young Cho,[§] Myung-Hyun Ryou,*[,†] and Yong Min Lee*[,†]

[†]Department of Chemical and Biological Engineering, Hanbat National University, 125, Dongseo-daero, Yuseong-gu, Daejeon 305-719, Republic of Korea

[‡]Intelligent Polymer Research Institute, ARC Centre of Excellence for Electromaterials Science, AIIM Facility, Innovation Campus, University of Wollongong, Wollongong, NSW 2522, Australia

[§]Division of Advanced Materials Engineering, Kongju National University, 275, Budae-dong, Cheonan, Chungnam 331-717, Republic of Korea

Supporting Information

ABSTRACT: A highly adhesive and thermally stable copolyimide (P84) that is soluble in organic solvents is newly applied to silicon (Si) anodes for high energy density lithium-ion batteries. The Si anodes with the P84 binder deliver not only a little higher initial discharge capacity (2392 mAh g^{-1}), but also fairly improved Coulombic efficiency (71.2%) compared with the Si anode using conventional polyvinylidene fluoride binder (2148 mAh g^{-1} and 61.2%, respectively), even though P84 is reduced irreversibly during the first charging process. This reduction behavior of P84 was systematically confirmed by cyclic voltammetry and Fourier-transform infrared analysis in attenuated total reflection mode of the Si anodes at differently charged voltages. The Si anode with P84 also shows ultrastable long-term cycle performance of 1313 mAh g^{-1} after 300 cycles at 1.2 A g^{-1} and 25 °C. From the morphological analysis on the basis of scanning electron microscopy and optical images and of the electrode adhesion properties determined by surface and interfacial cutting analysis system and peel tests, it was found that the P84 binder functions well and maintains the mechanical integrity of Si anodes during hundreds of cycles. As a result, when the loading level of the Si anode is increased from 0.2 to 0.6 mg cm^{-2}, which is a commercially acceptable level, the Si anode could deliver 647 mAh g^{-1} until the 300th cycle, which is still two times higher than the theoretical capacity of graphite at 372 mAh g^{-1}.

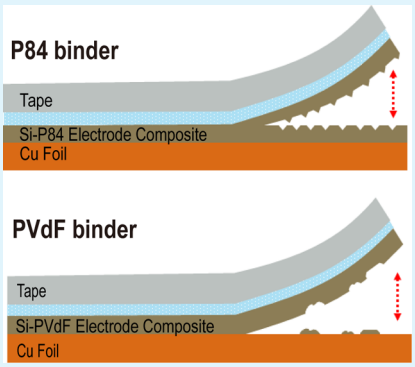

KEYWORDS: *copolyimide, polyvinylidene fluoride, polymeric binder, adhesion property, silicon, surface and interfacial cutting analysis system, peel test, lithium-ion batteries*

INTRODUCTION

The applications of lithium-ion batteries (LIBs) are expanding from portable electronic devices to electric vehicles (EVs) and energy-storage systems (ESSs). Large-scale LIBs for EVs and ESSs require considerably higher energy densities, shorter charging times, longer cycle lives, and lower cost per kilowatt-hour (kWh) than achieved until now.[1−3] Among these various requirements, high energy density is the most important, as the gravimetric and volumetric energy densities are closely related to vehicle mileage and price. As a result, numerous researchers have focused on developing new high-capacity electrode materials and electrolytes that are more reliable.[4−6] In particular, Si is a promising candidate as anode material owing to its high theoretical specific capacity of 3500 mAh g^{-1}, which is approximately 10-times the gravimetric capacity of conventional graphite-based anodes.[7,8] However, Si anodes have not been widely introduced into commercial LIBs because they experience large volume expansion (~400%) during the Li^+ insertion and extraction processes.[9] Moreover, this triggers pulverization of the Si particles, which then continually forms a new solid electrolyte interphase (SEI) layer on the exposed Si surface through an electrolytic decomposition reaction, thereby breaking the electrical pathways between Si particles, electrical conductors, and current collectors.[10−14] As a result, a serious capacity loss occurs immediately after a few cycles. To solve these problems of the Si anode, nanoscale Si particles with sizes below a few hundred nanometers have been studied extensively because smaller particles (~150 nm) effectively alleviate the volume expansion.[15,16] In addition, novel nanostructured Si materials have been synthesized by various methods to suppress the structural collapse caused by volume expansion.[17−21] Despite their enhanced electrochemical performance, the associated material-fabrication methods generally require complicated synthesis steps such as utilization/removal of

Received: April 19, 2015
Accepted: June 15, 2015
Published: June 15, 2015

DOI: 10.1021/acsami.5b03364
ACS Appl. Mater. Interfaces 2015, 7, 14851−14858

templates, time-consuming reactions, and high-temperature treatments. Therefore, the development of novel polymeric binders has been one of the challenging issues for next-generation LIBs.

Thus far, polyvinylidene fluoride (PVdF) has been widely utilized as a polymeric binder for commercialized LIBs over decades. Unfortunately, however, PVdF did not provide satisfactory cycling stability when applied to Si anodes due to its easy swelling property in electrolytes coupled with intrinsically low elasticity.[12,22−25] Recently, a number of studies have investigated the selection of appropriate polymeric binders, such as alginate,[26,27] poly(acrylic acid) (PAA),[12,25,28] carboxymethyl cellulose (CMC),[29] polyamide-imide (PAI),[30] and polyimide (PI) requiring thermal treatment at high temperature,[31−33] leading to dramatically enhanced electrochemical performance of Si anodes by changing only the kind of binder. Chemical structures of the typical polymeric binders are demonstrated in Figure 1. Considering the results, the enhanced mechanical properties are deemed to be the primary reason for improving the electrochemical performances.

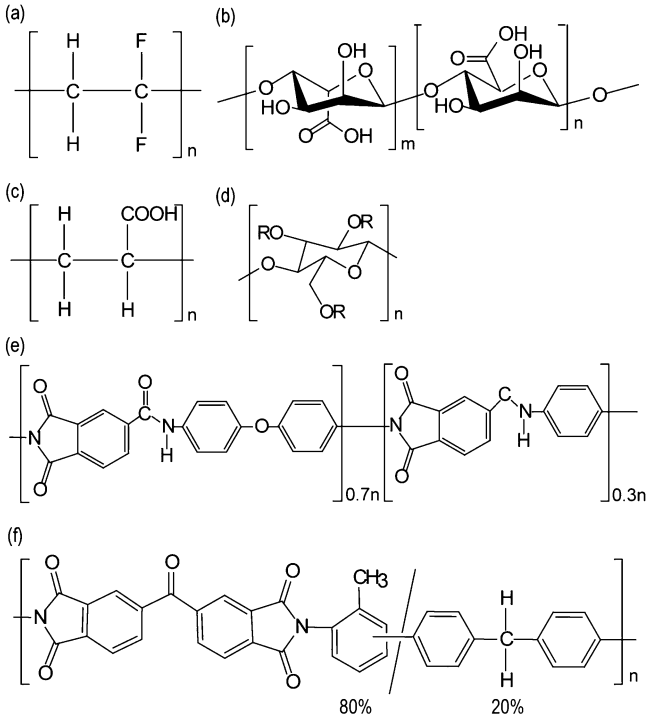

Figure 1. Molecular structures of typical polymeric binders for LIBs: (a) PVdF, (b) alginate, (c) PAA, (d) CMC, (e) PAI, and (f) P84 (copolyimide).

As an effort to develop a robust polymeric binder being easy to handle, in this work, we suggest the copolymerized polyimide 3,3,4,4-benzophenone-tetracarboxylic dianhydride (BTDA, P84) combined with 80% toluene diisocyanate (TDI) and 20% methylene diphenyl diisocyanate (MDI), which is soluble in various common solvents (such as *N*-methyl-2-pyrrolidone (NMP), *N*,*N*-dimethylformamide (DMF), and dimethylacetamide (DMAc)) and has outstanding mechanical properties. As an extension of our previous work in which P84 was used as separator-coating material,[34] and as thermally stable polymeric binder for the cathode,[35] in the present study, we investigated the electrochemical properties of P84 as polymeric binder for Si anodes and compared them to those of the PVdF system. We established the relationship between the adhesive properties of the polymeric binder and its electrochemical performance by using Fourier-transform infrared (FT-IR) spectroscopy, scanning electron microscopy (SEM), optical microscopy, peel tests, and surface and interfacial cutting analysis system (SAICAS).

EXPERIMENTAL SECTION

Electrode Preparation. Anodes were prepared by coating NMP (Sigma-Aldrich USA)-based slurry consisting of 60 wt % Si nanoparticles (30 nm, KCC, South Korea), 20 wt % conductive carbon (Super-P, Timcal, Switzerland), and 20 wt % polymeric binder onto Cu current collector foil (20 μm, Iljin Materials, South Korea) using a doctor blade. Two polymer binders were used: (i) PVdF (KF-1300, Kureha Battery Materials Co., Japan, Mw = 350 000) and (i) copolyimide (P84, HP Polymer GmbH, Austria, Mw = 150 000) in NMP. The cast slurry was dried in a vacuum oven at 60 °C for 2 h and then roll-pressed with a gap-control-type roll-pressing machine (CLP-2025, CIS, South Korea). The loading amount of Si was controlled to be 0.2 mg cm^{-2} for all the data shown in this paper for P84 and PVdF, except Figure 11 (high loading case), for which the loading of 0.6 mg cm^{-2} has been adopted.

Cell Assembly. The anodes employing PVdF and P84 binder were cut into disk shapes (diameter: 12 mm) and assembled into 2032-type coin half cells using Li metal (thickness, 450 μm; diameter, 16.2 mm; Honjo Metal Co., Japan) as counter electrode and polyethylene (PE) separator (thickness, 20 μm; diameter, 18 mm; ND420, Asahi Kasei E-materials, Japan), which was soaked with liquid electrolyte (1.15 M $LiPF_6$ in EC/EMC (30/70 by vol %)) containing 5 wt % fluoroethylene carbonate (FEC, PANAX ETEC) in an Ar-filled glovebox, in which the dew point was maintained at less than −80 °C.

Electrochemical Testing. After they were aged for 12 h, the coin cells were cycled as a formation step between 0.05 and 2.0 V at the constant current density of 0.2 A g^{-1} at 25 °C on both charging and discharging using a TOSCAT-3000U (Toyo System Co., Ltd., Japan). To evaluate the cyclability, the cells were cycled at the current density of 1.2 A g^{-1} for 300 cycles at 25 °C and, additionally, at several different current densities varying from 1.2−16.8 A g^{-1} for establishing the rate capability. To confirm the reversibility of the Si anode and the side reaction between polymeric binder and Li^+ during the charge−discharge processes, cyclic voltammetry (CV) was carried out using a VSP impedance analyzer (Biologic SAS, France). As-prepared coin cells (Si/Li metal) were scanned at a scan rate of 0.2 mV s^{-1} in the voltage range between 0.05 and 2 V versus Li/Li^+, starting from open-circuit voltage (OCV).

FT-IR Spectroscopy. FT-IR spectra of the Si anodes were analyzed to clarify the reaction mechanism of the polymeric binder with Li^+. Therefore, they were obtained at variously charged states including the fully discharged state from attenuated total reflection (ATR) measurements on the instrument FTIR 4200 (JASCO) with spectral resolution of 4 cm^{-1} in the frequency range of 400−4000 cm^{-1}. Each anode sample was prepared by the following procedure: after the cells reached a particular potential corresponding to a specific state-of-charge (SOC), they were carefully disassembled in a glovebox, and then the electrodes were rinsed in dimethyl carbonate (DMC) to remove residual electrolyte and subsequently dried in a vacuum chamber overnight.

Morphological Analysis of Anodes. Field-emission scanning electron microscopy (FE-SEM, S4800, Hitachi, Japan) and optical microscopy (SV-32, Sometech Vision, South Korea) were used to investigate the morphological changes of the Si anode surfaces.

Peel Test. A 19 mm wide and 20 mm long anode sample piece was attached to 3M adhesive tape, and its peel strength was measured with a micro material tester (Instron 5848, Instron Company, USA). The adhesive tape was removed by peeling at the angle of 90° at the constant displacement rate of 10 mm min^{-1}; the applied load was continuously measured, and force/displacement plots were produced. Before and after testing, the surface morphologies of the anode and tape were observed by optical microscopy.

DOI: 10.1021/acsami.5b03364
ACS Appl. Mater. Interfaces 2015, 7, 14851−14858

SAICAS Measurements. The shear stress of the electrodes and the adhesion strength between electrode and current collector were measured using a SAICAS (Daipla Wintes Co., Ltd., Japan). For the SAICAS measurements, a boron nitride blade (width: 1 mm) fixed at 45° shear angle was used. During the test, the blade moved in the horizontal direction at 1.0 μm s^{-1}, maintaining a vertical force of 0.2 N.

RESULTS AND DISCUSSION

The optical images shown in Figure 2 demonstrate the good solubility of P84 polymeric binder in various organic solvents

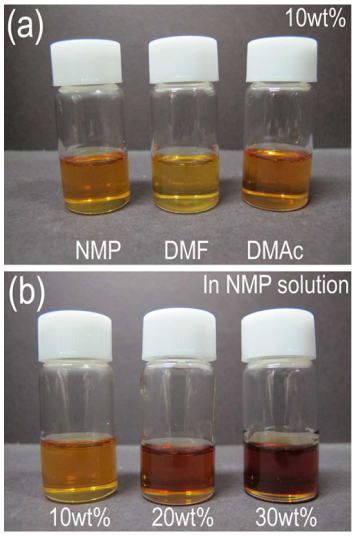

Figure 2. (a) 10 wt % P84 binder solutions in various organic solvents (NMP, DMF, and DMAc), (b) P84/NMP solutions with concentration of 10, 20, and 30 wt %.

such as NMP, DMF, and DMAc (Figure 2a). In particular, its high solubility of approximately 30 wt % in the representative LIB solvent NMP is a very attractive feature because the solid content in the slurry should be increased as much as possible to reduce both solvent usage and energy consumption for drying (Figure 2b). Moreover, unlike previous polyimide binder systems for LIBs, P84 does not need thermal treatment at 300 °C for a few hours to convert the polyamic acid to polyimide. Therefore, P84 as binder material can be easily embedded into the conventional battery manufacturing process.

Figure 3 presents the first charge−discharge curves of two half cells with different Si anodes; one was prepared with P84 binder and the other with the conventional PVdF binder as reference. At the beginning of the first charging, the P84 exhibits longer irreversible reaction in the region from OCV to

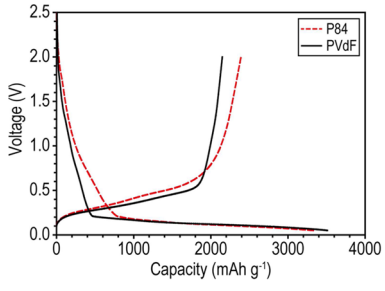

Figure 3. First charge−discharge voltage curves of two Si anodes having either PVdF or P84 binder (voltage range, 0.05−2.0 V vs Li/Li^+; current density, 0.2 A g^{-1}).

0.3 V, which must be related to some reduction reaction of P84. Therefore, the charged capacity of the half cell with P84 (3331 mAh g^{-1}) is a little lower than that of the half cell with PVdF (3511 mAh g^{-1}). However, the discharge capacity of the half cell with P84 is approximately 2392 mAh g^{-1}, which is approximately 10% (244 mAh g^{-1}) higher than that of the reference cell (2148 mAh g^{-1}). As a result, the initial Coulombic efficiency could be enhanced from 61.2% to 71.2%, thereby revealing that polymeric binder can affect the electrochemical properties of Si anodes. To verify the longer irreversible reaction of the half cell with P84 appearing from OCV to 0.3 V, we performed additional CV experiments shown in Figure 4, panels a and b.

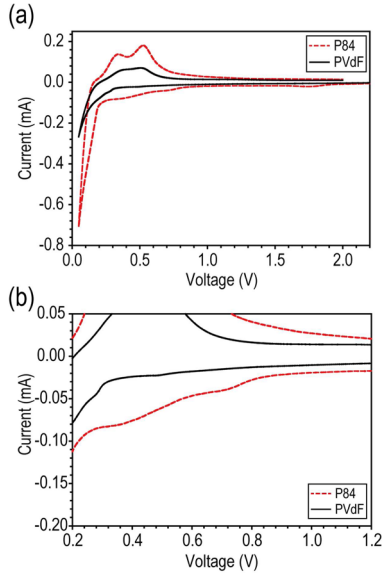

Figure 4. (a) Cyclic voltammogram of the PVdF and P84 electrodes between 0.05 and 2.0 V (vs Li/Li^+) at 0.2 mV s^{-1} and 25 °C, and (b) magnified region of panel a.

As is evident from Figure 4, the PVdF cell exhibited the typical CV behavior of a Si anode, and there was no appreciable capacity in the voltage range of the SEI formation between 0.5 and 0.7 V versus Li/Li^+ for PVdF,[36] which could possibly be small amount of capacity involved in SEI compared to the high charge capacity we observed. In contrast, the P84 cell showed a broad and high reduction peak possibly representing a characteristic property of P84, which will be proved in the next section. The reduction peak between 0.2 and 0.05 V related to Li−Si alloy not only remains, but also even increases. This irreversible reduction reaction of P84 is deemed to play a prominent role in Si anodes having large volume expansion. Moreover, since the P84 reduction does not occur in the subsequent cycles, we need not be concerned about continuous decomposition of P84. There were sharp Li insertion reaction peaks near 0 V versus Li/Li^+. It is reported that amorphous Si reacts with Li at slightly higher potential (~220 mV) than crystalline Si (~120 mV).[37] Thus, the ratio between amorphous and crystalline structure of Si would determine the specific Li insertion potential (see also Figure S1 in the Supporting Information).

To unveil the reaction mechanism, FT-IR analyses were conducted at various potentials (pristine electrode, 1.0 V, 0.7 V, 0.3 V, 0.1 V, and fully discharged state vs Li/Li^+) and are

DOI: 10.1021/acsami.5b03364
ACS Appl. Mater. Interfaces 2015, 7, 14851−14858

presented in Figure 5. C═O stretching (1800 and 1760 cm^{-1}) and C−N−C stretching (1360 cm^{-1}) peaks of imide rings in

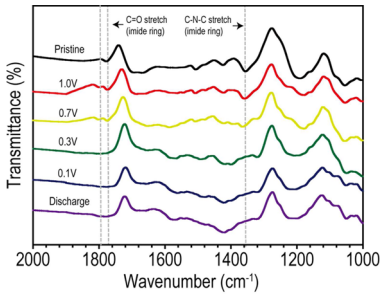

Figure 5. FT-IR spectra of the P84 electrodes at various potentials (pristine electrode, 1.0, 0.7, 0.3, 0.1 V vs Li/Li^+, and fully discharged state).

P84 are clearly observed in the pristine Si anode. However, when the voltage was lowered to 0.3 V, those characteristic peaks changed; the C═O stretching peaks disappeared, and the C−N−C stretching peak shifted from 1360 to 1420 cm^{-1}. This phenomenon is quite similarly observed in the electrochemical reaction of the PAI binder system.[30] As suggested by the previous work,[30] the C═O group of the imide ring in P84 reacts with Li^+ during charging, and this process seems to positively influence the electrochemical performance of Si anodes.

For the morphological analysis of the Si anodes with different binders, we gathered SEM and optical microscopic images of the electrode surfaces at different electrochemical states such as pristine, fully charged, and fully discharged. Although different polymeric binders are used, the surface morphology of the electrodes in their pristine state seems to be very similar (Figure 6a,b), characterized by a large number of pores between agglomerated nanosized Si particles. However, while either charging or discharging is progressed, their surface morphology changes distinctly, depending on the binder type. When fully charged, the two investigated types of electrodes become fully packed due to the volume expansion of Si and some decomposition products. However, although a large number of original Si particles are discernible in the fully charged PVdF electrode, most of the Si particles in the P84 electrode merged into micron-sized clusters (Figure 6c,d). This difference may be related to the reduction reaction of P84 during the first charging process. After both types of Si anodes have been fully discharged (delithiated), the P84 electrode is much more robust against mechanical stress during subsequent charging and discharging, resulting in very small, submicron-sized cracks, whereas the PVdF electrode contains huge cracks (Figure 5e,f). Moreover, the surface of the Cu current collector could be seen through the cracks in the PVdF electrode. From the lower magnified SEM images (Figure 6g,h), it is evident that the P84 electrode shows more stable dimensional stability. This phenomenon is also confirmed by the optical images of the two P84 and PVdF electrodes at fully charged and discharged states (Figure S2 in the Supporting Information). Thus, P84 could provide the Si anode with high mechanical stability to withstand the volume changes of Si.

To investigate the effects of the binder on the electrochemical performance, namely cycle life and rate capability, two half cells using either P84 or PVdF were fabricated, as mentioned in the Experimental Section. As shown in Figure 7,

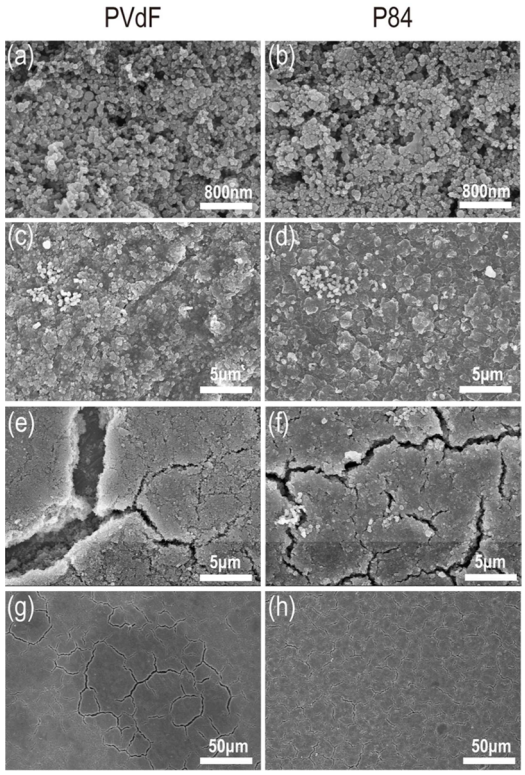

Figure 6. SEM images of Si anodes at (a, b) pristine, (c, d) fully charged, and (e, f) fully discharged states. (g, h) Lower magnified images of panels e and f at fully discharged state.

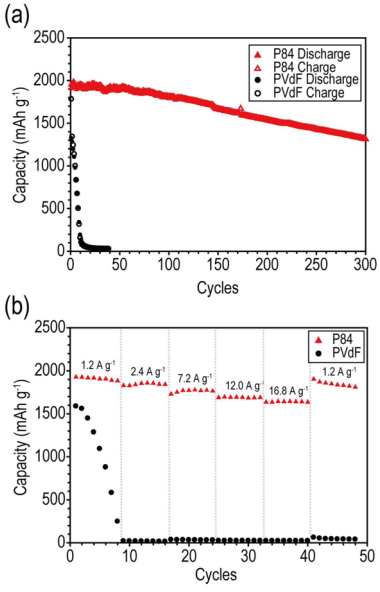

Figure 7. (a) Cycle performance of the PVdF and P84 electrodes operated at a current density of 1.2 A g^{-1} for 300 cycles at 25 °C. (b) Rate capability of the PVdF and P84 electrodes cycled at different current densities from 1.2−16.8 A g^{-1}.

panel a, the P84 cell shows a quite high specific capacity of around 1903 mAh g^{-1} even at 1.2 A g^{-1} at the beginning of cycling. Furthermore, it maintains its capacity resulting in 1313 mAh g^{-1} after 300 cycles at 25 °C with almost 99% Coulombic efficiencies. On the other hand, the capacity of the PVdF cell drops too quickly to be used as secondary battery. Along with numerous previous works on Si anodes with PVdF binder, this

DOI: 10.1021/acsami.5b03364
ACS Appl. Mater. Interfaces 2015, 7, 14851−14858

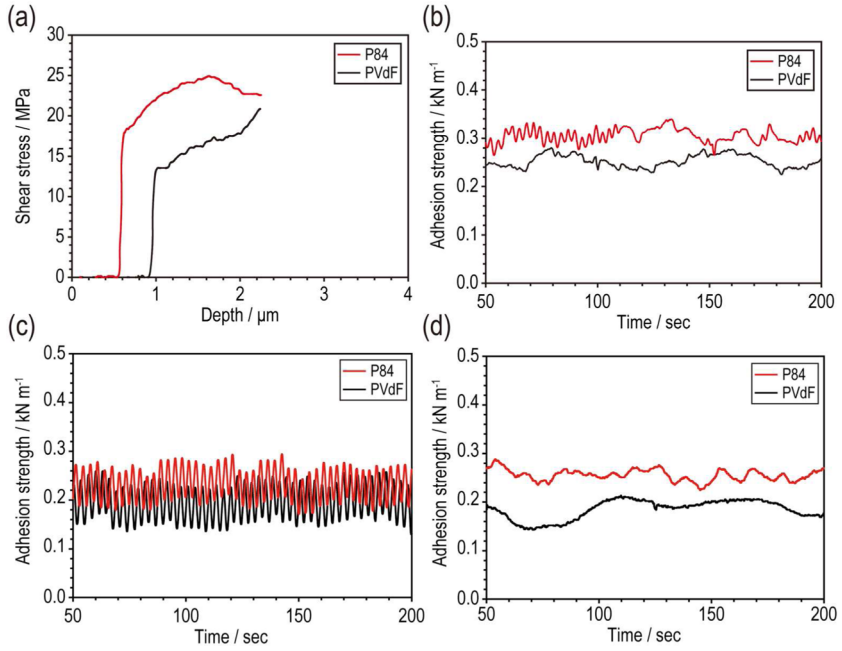

Figure 8. (a) Shear stress (vs depth) of PVdF and P84 electrodes during the cutting mode in SAICAS. Adhesion strength (vs time) of PVdF and P84 electrodes during the peeling mode in SAICAS (b) before and (c) after 10 cyclings (0.05 and 2 V vs Li/Li^+ at a current density of 1.2 A g^{-1} at 25 °C associated with Figure 7b). (d) Adhesion strength (vs time) of PVdF and P84 during the peeling mode at mid-depths (7 μm from the current collector).

poor cycle performance must be closely related to the insufficient binding ability, that is, van der Waals interaction, of PVdF toward Si nanoparticles and current collectors.[12,22−25] The rate capability of the two cells was evaluated by changing the current density from 1.2 A g^{-1} to 16.8 A g^{-1}, presented in Figure 7, panel b. Considering the first discharge capacity of the P84 electrode of around 1929 mAh g^{-1} (at 1.2 A g^{-1}) as the practical capacity, the current density of 16.8 A g^{-1} is the current rate to fully discharge the electrode within approximately 7 min (9C rate). Even at that high rate, the P84 cell maintains approximately 86% of its original capacity, specifically 1636 mAh g^{-1}, which is high enough to be applied in high-power LIBs. However, the PVdF cell could not survive under the mildest current density because of the poor structural stability of the electrode against electrochemical stress.

For the quantitative evaluation of the mechanical strength of Si anodes, we measured their adhesion properties by using the new and delicate SAICAS instrument along with the conventional peeling test. As already explained and demonstrated in previous studies applying SAICAS to LIB electrodes, the shear stress and adhesion strength at a specific interface can be obtained by this method.[35,38] As presented in Figure 8, panel a, the shear stress, corresponding to the force needed to cut the same area through the electrode layer, of the P84 electrode is approximately 22% higher than that of the PVdF electrode (18.0 MPa vs 14.7 MPa). In addition, since the shear stress of the P84 electrode starts to increase earlier than in case of the PVdF electrode, P84 may result in a more rigid and robust electrode surface. While the shear-stress information can be obtained in cutting mode, the peeling mode reveals the adhesion strength of the electrodes at various depths. Similar to the shear strength behavior, the adhesion strength of the P84 electrode is approximately 20% higher comparing either the maximum (0.339 kN m^{-1} vs 0.280 kN m^{-1}) or the average values (0.306 kN m^{-1} vs 0.252 kN m^{-1}) (Figure 8b). Furthermore, as demonstrated in Figure 8, panel c, the adhesion strengths of the P84 and the PVdF electrodes were measured after 10 cycles of operation (0.05 and 2 V vs Li/Li^+ at a current density of 1.2 A g^{-1} at 25 °C). The average values of adhesion strength of P84 (0.231 kN m^{-1}) were higher than those of PVdF (0.195 kN m^{-1}). Figure 8, panel d describes the adhesion strength of P84 and PVdF measured at midheight. Again, P84 (0.237 kN m^{-1}) revealed a relatively higher value compared to PVdF (0.191 kN m^{-1}). Considering the results, we could infer that intrinsic adhesion strength of P84 is contributed to the higher mechanical strength between Si particles and between Si electrode and Cu foil as well. Consequently, the P84 binder greatly contributes to the mechanical stability of the composite Si anode withstanding severe mechanical stress during charging and discharging.

We repeated the adhesion-property measurements through the conventional peel test to identify the detachment behavior at the surface. From Figure 9 exhibiting the load (adhesion strength) profiles versus displacements, the adhesion strength of the P84 electrode at the surface is much higher than that of the PVdF electrode, namely by approximately 300% (0.479 kN

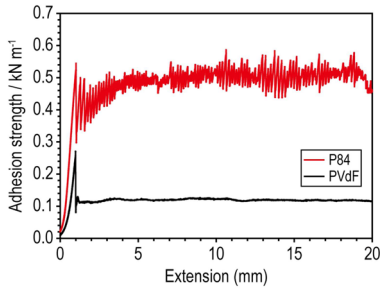

Figure 9. Adhesion strength profiles of PVdF and P84 electrodes during the peel test.

DOI: 10.1021/acsami.5b03364
ACS Appl. Mater. Interfaces 2015, 7, 14851−14858

m^{-1} vs 0.118 kN m^{-1}, respectively). Compared to the corresponding adhesion strengths determined by SAICAS, in which the P84 electrode has only approximately 20% higher strength, the binder P84 plays a more prominent role at the surface than inside of the electrode and at the current collector interface. In addition, the profile of the P84 electrode strongly exhibits a large number of adhesive points arising from load fluctuations during the peeling period, whereas the PVdF electrode shows an almost constant adhesion strength value of approximately 0.118 kN m^{-1} in the same period. After the peel test, we compared the surface morphologies of the two Si anodes by optical microscopy. As described in Figure 10, panels

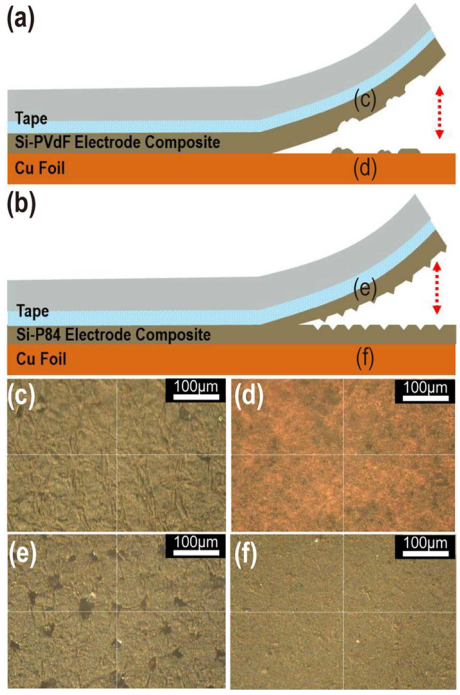

Figure 10. (a, b) Schematics illustrating the peel test of the PVdF and P84 electrodes. (c, d) Tape and Cu foil sides of PVdF electrodes after the peel test. (e, f) Tape and Cu foil sides of P84 electrodes after the peel test.

a and b, the PVdF electrode layer is totally peeled off from the Cu current collector and transferred onto the 3M-tape surface (Figure 10c,d). However, a significant portion of the P84 electrode remains on the Cu current collector even after peeling (Figure 10e,f), which indicates the significantly enhanced adhesion properties of the P84 electrode. Some evidence of the adhesion mechanism of P84 is provided from the detached surface morphology. Since the P84 electrode surface is detached onto the tape at various dots (Figure 10e), we can infer that the P84 binder might exist in some localized regions. This result well agrees with the peel test and our previous work on P84-coated separator,[34] in which the spherical shape of P84 could be found after evaporation of the solvent from the P84 solution.

The effect of the P84 binder on the Si anode was further investigated by increasing the electrode loading from 0.2 to 0.6 mg cm^{-2} with associated areal capacity comparable to that of conventional graphite electrodes of 2 mAh cm^{-2}. While the highly loaded PVdF electrode shows not only lower initial discharge capacity (2148 → 1409 mAh g^{-1}), but also poor Coulombic efficiency (61.2 → 46.7%), the P84 electrode at high loading level maintains its original values (2392 → 2130 mAh g^{-1}, 71.2 → 69.7%, respectively) quite well (Figure 11a).

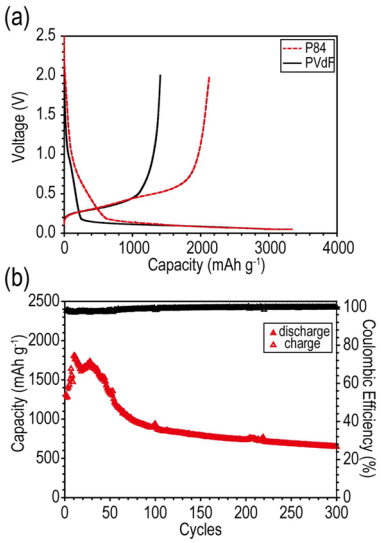

Figure 11. (a) First charge−discharge voltage curves of two Si anodes (PVdF and P84 binders) with a high loading of 0.6 mg cm^{-2}. (b) Cycling capacities and Coulombic efficiencies of the P84 electrode with high loading at a current density of 1.2 A g^{-1} for 300 cycles.

The cycle life is also compared in Figure 11, panel b. The P84 electrode shows a quite high specific capacity of approximately 647 mAh g^{-1} until the 300th cycle, which is two times higher than the theoretical capacity of graphite (372 mAh g^{-1}). However, interestingly, the discharge capacity is gradually increased during the initial 30 cycles and then decreased and stabilized. This peculiar behavior seems to be closely related to the excellent binding ability of P84 to activate some electrochemically inactive Si nanoparticles. Therefore, we believe that the binding property found in P84 is most essential for Si anodes in commercial LIBs.

CONCLUSIONS

We have successfully introduced a new polymeric binder, copolyimide (P84), for Si anodes in LIBs. In comparison with the conventional PVdF binder, the Si with P84 showed good initial electrochemical properties, in particular higher discharge capacity and Coulombic efficiency. However, P84 is reduced irreversibly in the first charging process. The long-term cycle performance was greatly improved and delivered 1313 mAh g^{-1} after 300 cycles at 1.2 A g^{-1} and 25 °C, which is ascribed to the superior adhesion property of P84 confirmed by SAICAS, peel test, and morphological images. From this result, we conclude that the P84 binder can alleviate effectively the deterioration of the electrochemical properties originating from the volume expansion of the Si anode. Therefore, P84 represents a promising polymeric binder for the active material of high-capacity LIBs, which suffer from the large volume expansion during the charge−discharge process.

ASSOCIATED CONTENT

Supporting Information

CV results and optic images of the PVdF and the P84 electrodes, respectively. The Supporting Information is available free of charge on the ACS Publications website at DOI: 10.1021/acsami.5b03364.

DOI: 10.1021/acsami.5b03364
ACS Appl. Mater. Interfaces 2015, 7, 14851−14858

AUTHOR INFORMATION

Corresponding Authors

*E-mail: mhryou@hanbat.ac.kr. Phone: +82-42-821-1534. Fax: +82-42-821-1692.

*E-mail: yongmin.lee@hanbat.ac.kr. Phone: +82-42-821-1549. Fax: +82-42-821-1692.

Author Contributions

⊥These authors contributed equally to this work.

Notes

The authors declare no competing financial interest.

ACKNOWLEDGMENTS

This research was supported by Basic Science Research Program through the National Research Foundation of Korea (NRF) funded by the Ministry of Science, ICT & Future Planning (2014R1A1A1005861). This research was also financially supported by the Ministry of Education (MOE) and National Research Foundation of Korea (NRF) through the Human Resource Training Project for Regional Innovation (No. 2014066977).

REFERENCES

(1) Hassoun, J.; Panero, S.; Reale, P.; Scrosati, B. A New, Safe, High-Rate, and High-Energy Polymer Lithium-Ion Battery. *Adv. Mater.* **2009**, *21*, 4807−4810.

(2) Armand, M.; Tarascon, J.-M. Building Better Batteries. *Nature* **2008**, *451*, 652−657.

(3) Chu, S.; Majumdar, A. Opportunities and Challenges for a Sustainable Energy Future. *Nature* **2012**, *488*, 294−303.

(4) Song, Y.-M.; Han, J.-G.; Park, S.; Lee, K. T.; Choi, N.-S. A Multifunctional Phosphite-Containing Electrolyte for 5 V-Class $LiNi_{0.5}Mn_{1.5}O_4$ Cathodes with Superior Electrochemical Performance. *J. Mater. Chem. A* **2014**, *2*, 9506−9513.

(5) Xia, H.; Meng, Y.; Lu, L.; Ceder, G. Electrochemical Properties of Nonstoichiometric $LiNi_{0.5}Mn_{1.5}O_{4-\delta}$ Thin-Film Electrodes Prepared by Pulsed Laser Deposition. *J. Electrochem. Soc.* **2007**, *154*, A737−A743.

(6) Choi, N.-S.; Han, J.-G.; Ha, S.-Y.; Park, I.; Back, C.-K. Recent Advances in the Electrolytes for Interfacial Stability of High-Voltage Cathodes in Lithium-Ion Batteries. *RSC Adv.* **2015**, *5*, 2732−2748.

(7) Obrovac, M.; Christensen, L. Structural Changes in Silicon Anodes during Lithium Insertion/Extraction. *Electrochem. Solid State Lett.* **2004**, *7*, A93−A96.

(8) Liu, X. H.; Zhang, L. Q.; Zhong, L.; Liu, Y.; Zheng, H.; Wang, J. W.; Cho, J.-H.; Dayeh, S. A.; Picraux, S. T.; Sullivan, J. P. Ultrafast Electrochemical Lithiation of Individual Si Nanowire Anodes. *Nano Lett.* **2011**, *11*, 2251−2258.

(9) Kasavajjula, U.; Wang, C.; Appleby, A. J. Nano- and Bulk-Silicon-Based Insertion Anodes for Lithium-Ion Secondary Cells. *J. Power Sources* **2007**, *163*, 1003−1039.

(10) Lee, Y. M.; Lee, J. Y.; Shim, H.-T.; Lee, J. K.; Park, J.-K. SEI Layer Formation on Amorphous Si Thin Electrode during Precycling. *J. Electrochem. Soc.* **2007**, *154*, A515−A519.

(11) Zhang, W.-J. A Review of the Electrochemical Performance of Alloy Anodes for Lithium-Ion Batteries. *J. Power Sources* **2011**, *196*, 13−24.

(12) Magasinski, A.; Zdyrko, B.; Kovalenko, I.; Hertzberg, B.; Burtovyy, R.; Huebner, C. F.; Fuller, T. F.; Luzinov, I.; Yushin, G. Toward Efficient Binders for Li-Ion Battery Si-Based Anodes: Polyacrylic Acid. *ACS Appl. Mater. Interfaces* **2010**, *2*, 3004−3010.

(13) Kim, H.; Seo, M.; Park, M. H.; Cho, J. A Critical Size of Silicon Nano-Anodes for Lithium Rechargeable Batteries. *Angew. Chem.* **2010**, *49*, 2146−2149.

(14) Xue, L.; Xu, G.; Li, Y.; Li, S.; Fu, K.; Shi, Q.; Zhang, X. Carbon-Coated Si Nanoparticles Dispersed in Carbon Nanotube Networks as Anode Material for Lithium-Ion Batteries. *ACS Appl. Mater. Interfaces* **2012**, *5*, 21−25.

(15) Liu, X. H.; Zhong, L.; Huang, S.; Mao, S. X.; Zhu, T.; Huang, J. Y. Size-Dependent Fracture of Silicon Nanoparticles during Lithiation. *ACS Nano* **2012**, *6*, 1522−1531.

(16) Song, T.; Xia, J.; Lee, J.-H.; Lee, D. H.; Kwon, M.-S.; Choi, J.-M.; Wu, J.; Doo, S. K.; Chang, H.; Park, W. I. Arrays of Sealed Silicon Nanotubes as Anodes for Lithium-Ion Batteries. *Nano Lett.* **2010**, *10*, 1710−1716.

(17) Lee, D. J.; Lee, H.; Ryou, M.-H.; Han, G.-B.; Lee, J.-N.; Song, J.; Choi, J.; Cho, K. Y.; Lee, Y. M.; Park, J.-K. Electrospun Three-Dimensional Mesoporous Silicon Nanofibers as an Anode Material for High-Performance Lithium Secondary Batteries. *ACS Appl. Mater. Interfaces* **2013**, *5*, 12005−12010.

(18) Wu, H.; Chan, G.; Choi, J. W.; Yao, Y.; McDowell, M. T.; Lee, S. W.; Jackson, A.; Yang, Y.; Hu, L.; Cui, Y. Stable Cycling of Double-Walled Silicon Nanotube Battery Anodes through Solid−Electrolyte Interphase Control. *Nat. Nanotechnol.* **2012**, *7*, 310−315.

(19) Chen, Y.; Zeng, S.; Qian, J.; Wang, Y.; Cao, Y.; Yang, H.; Ai, X. Li^+-Conductive Polymer-Embedded Nano-Si Particles as Anode Material for Advanced Li-Ion Batteries. *ACS Appl. Mater. Interfaces* **2014**, *6*, 3508−3512.

(20) Jung, D. S.; Hwang, T. H.; Park, S. B.; Choi, J. W. Spray Drying Method for Large-Scale and High-Performance Silicon Negative Electrodes in Li-Ion Batteries. *Nano Lett.* **2013**, *13*, 2092−2097.

(21) Hwang, T. H.; Lee, Y. M.; Kong, B.-S.; Seo, J.-S.; Choi, J. W. Electrospun Core−Shell Fibers for Robust Silicon Nanoparticle-Based Lithium Ion Battery Anodes. *Nano Lett.* **2012**, *12*, 802−807.

(22) Park, S.-J.; Zhao, H.; Ai, G.; Wang, C.; Song, X.; Yuca, N.; Battaglia, V. S.; Yang, W.; Liu, G. Side-Chain Conducting and Phase-Separated Polymeric Binders for High-Performance Silicon Anodes in Lithium-Ion Batteries. *J. Am. Chem. Soc.* **2015**, *137*, 2565−2571.

(23) Koo, B.; Kim, H.; Cho, Y.; Lee, K. T.; Choi, N. S.; Cho, J. A Highly Cross-Linked Polymeric Binder for High-Performance Silicon Negative Electrodes in Lithium-Ion Batteries. *Angew. Chem.* **2012**, *51*, 8762−8767.

(24) Hochgatterer, N.; Schweiger, M.; Koller, S.; Raimann, P.; Wöhrle, T.; Wurm, C.; Winter, M. Silicon/Graphite Composite Electrodes for High-Capacity Anodes: Influence of Binder Chemistry on Cycling Stability. *Electrochem. Solid State Lett.* **2008**, *11*, A76−A80.

(25) Komaba, S.; Shimomura, K.; Yabuuchi, N.; Ozeki, T.; Yui, H.; Konno, K. Study on Polymer Binders for High-Capacity SiO Negative Electrode of Li-Ion Batteries. *J. Phys. Chem. C* **2011**, *115*, 13487−13495.

(26) Ryou, M. H.; Kim, J.; Lee, I.; Kim, S.; Jeong, Y. K.; Hong, S.; Ryu, J. H.; Kim, T. S.; Park, J. K.; Lee, H. Mussel-Inspired Adhesive Binders for High-Performance Silicon Nanoparticle Anodes in Lithium-Ion Batteries. *Adv. Mater.* **2013**, *25*, 1571−1576.

(27) Kovalenko, I.; Zdyrko, B.; Magasinski, A.; Hertzberg, B.; Milicev, Z.; Burtovyy, R.; Luzinov, I.; Yushin, G. A Major Constituent of Brown Algae for Use in High-Capacity Li-Ion Batteries. *Science* **2011**, *334*, 75−79.

(28) Yabuuchi, N.; Shimomura, K.; Shimbe, Y.; Ozeki, T.; Son, J. Y.; Oji, H.; Katayama, Y.; Miura, T.; Komaba, S. Graphite-Silicon-Polyacrylate Negative Electrodes in Ionic Liquid Electrolyte for Safer Rechargeable Li-Ion Batteries. *Adv. Energy Mater.* **2011**, *1*, 759−765.

(29) Lestriez, B.; Bahri, S.; Sandu, I.; Roué, L.; Guyomard, D. On the Binding Mechanism of CMC in Si Negative Electrodes for Li-Ion Batteries. *Electrochem. Commun.* **2007**, *9*, 2801−2806.

(30) Choi, N.-S.; Yew, K. H.; Choi, W.-U.; Kim, S.-S. Enhanced Electrochemical Properties of a Si-Based Anode Using an Electrochemically Active Polyamide Imide Binder. *J. Power Sources* **2008**, *177*, 590−594.

(31) Yuan, Q.; Zhao, F.; Zhao, Y.; Liang, Z.; Yan, D. Reason Analysis for Graphite-Si/SiO_x/C Composite Anode Cycle Fading and Cycle Improvement with PI Binder. *J. Solid State Electrochem.* **2014**, *18*, 2167−2174.

(32) Kim, J. S.; Choi, W.; Cho, K. Y.; Byun, D.; Lim, J.; Lee, J. K. Effect of Polyimide Binder on Electrochemical Characteristics of

DOI: 10.1021/acsami.5b03364
ACS Appl. Mater. Interfaces 2015, 7, 14851−14858

Surface-Modified Silicon Anode for Lithium-Ion Batteries. *J. Power Sources* **2013**, *244*, 521−526.
(33) Jeong, G.; Lee, S. M.; Choi, N. S.; Kim, Y.-U.; Lee, C. K. Stabilizing Dimensional Changes in Si-Based Composite Electrodes by Controlling the Electrode Porosity: An in Situ Electrochemical Dilatometric Study. *Electrochim. Acta* **2011**, *56*, 5095−5101.
(34) Song, J.; Ryou, M.-H.; Son, B.; Lee, J.-N.; Lee, D. J.; Lee, Y. M.; Choi, J. W.; Park, J.-K. Copolyimide-Coated Polyethylene Separators for Enhanced Thermal Stability of Lithium-Ion Batteries. *Electrochim. Acta* **2012**, *85*, 524−530.
(35) Choi, J.; Ryou, M.-H.; Son, B.; Song, J.; Park, J.-K.; Cho, K. Y.; Lee, Y. M. Improved High-Temperature Performance of Lithium-Ion Batteries through Use of a Thermally Stable Copolyimide-Based Cathode Binder. *J. Power Sources* **2014**, *252*, 138−143.
(36) Graetz, J.; Ahn, C.; Yazami, R.; Fultz, B. Highly Reversible Lithium Storage in Nanostructured Silicon. *Electrochem. Solid State Lett.* **2003**, *6*, A194−A197.
(37) Cui, L.-F.; Ruffo, R.; Chan, C. K.; Peng, H.; Cui, Y. Crystalline-Amorphous Core−Shell Silicon Nanowires for High Capacity and High Current Battery Electrodes. *Nano Lett.* **2008**, *9*, 491−495.
(38) Son, B.; Ryou, M.-H.; Choi, J.; Lee, T.; Yu, H. K.; Kim, J. H.; Lee, Y. M. Measurement and Analysis of Adhesion Property of Lithium Ion Battery Electrodes with SAICAS. *ACS Appl. Mater. Interfaces* **2013**, *6*, 526−531.

DOI: 10.1021/acsami.5b03364
ACS Appl. Mater. Interfaces 2015, 7, 14851−14858